Planar Feeding Circuit Integrated With a Compact Dielectric Resonator for Polarization Diversity

Planar Feeding Circuit Integrated With a Compact Dielectric Resonator for Polarization Diversity

Maksim V. Kuznetcov, *Graduate Student Member, IEEE*, Symon K. Podilchak, *Member, IEEE*, Jonathan C. Johnstone, *Member, IEEE*, Michel Clénet, *Senior Member, IEEE*, and Yahia M. M. Antar, *Life Fellow, IEEE*

***Abstract*— A compact two-port feeding circuit that supports a dielectric resonator (DR) element is presented for applications requiring polarization diversity. The L-band structure consists of a cylindrical DR that can generate right-handed circular polarization (RHCP), left-handed circular polarization (LHCP), and linearly polarized radiation. The DR dimensions have been optimized considering a relative dielectric constant of $\epsilon_r = 27$, and the entire structure (the circuit and DR) has dimensions of 9 cm × 9 cm × 2 cm (or about 0.3 λ_0 × 0.3 λ_0 × 0.07 λ_0 at the lower operational frequency range). Radiation by the DR originates from four orthogonal $HE_{11\delta}$ modes that are excited by four radial slots etched out of the ground plane (all underneath the DR) printed on top of an FR-4 substrate. Each of these four slots is unconventionally driven by two 50-Ω microstrip lines, and all four radial slots conform to the shape of the top cylindrical DR element. Polarization diversity is achieved with this DR and circuit system (DRCS) arrangement, mainly by the design of its fully integrated and planar circuit, which routes power to the eight microstrip lines for DR excitation. This FR-4 printed circuit board (PCB) feeding system consists of two meandered Wilkinson power dividers, two 180° delay lines, and four surface mount 90° hybrid couplers. The complete DRCS is compact in size, is broadband (more than 40%), and offers the advantage of requiring only two external ports, one for LHCP the other for RHCP, while an external phase shifter and a combiner are needed for linearly polarized radiation.**

***Index Terms*— Antenna feeds, aperture coupled slots (ACSs), dielectric resonator antenna (DRA), hybrid antenna, polarization diversity.**

I. Introduction

With the development of new circuit technologies, high dielectric materials, and new fabrication approaches, clever ways for dielectric resonator antenna (DRA) implementations have been examined. These structures are popular due to their high degree of freedom in the design and possible feeding techniques while offering high gain, low loss, and good matching over frequency. The flexibility of the design also extends to the dielectric radiating elements themselves, in which new shapes can provide more flexibility, achieving different features. Some recent developments include the segmented hemispheric shape [1], the stair-shape [2], and the Z-shape [3] DRs. Compared to more standard rectangular or cylindrical radiating elements, modified shapes can offer good matching and overall efficiency, while these features can be controlled during manufacturing.

One such design is the T-shape DR as in [4]. The structure consists of a T-shape resonator with a 50-Ω microstrip line on the bottom of the dielectric. This DR operated over an ultrawide bandwidth between 3.81 and 8.39 GHz, reaching a maximum gain of 7.35 dBi. Similarly, an S-shaped DR [5] with a substrate integrated waveguide (SIW) feeding system was presented. The structure consisted of an S-shape resonator placed on the cavity, which provided good impedance matching, low loss, and high efficiency between 23 and 33 GHz, while the maximum gain of the antenna was 6 dBi.

Other research studies on DRs are also focused on the feeding approach using resonator structures and circuit implementations that are easier to manufacture and design. For example, this could be one-port [6] or multiple-port [7] type feeding structures. Examples of feeding technologies include microstrip, probe-fed, coplanar waveguide, and SIW. Feeding techniques have also been extended to multi-in multi-out (MIMO) DR systems with multiple resonators achieving pattern diversity [8], [9].

When polarization control is of interest, DRs with one-port feeding generally offer one type of polarization, circular polarization (CP), or linear polarization (LP) in the far-field. Dual-port feed systems can also offer two or more polarization states. These types of dual-polarization systems can complicate the overall design, and if compact structures are desired, implementation challenges might arise. The choice of the feeding system and shape of the resonator also defines the operating modes, i.e., typical rectangular and cylindrical-type DR elements supporting TE, TM, HEM, and other hybrid modes [10], [11]. These radiating structures with high polarization diversity can also be of interest in modern communication systems. They can offer lower losses from multipath effects and offer the possibility to employ

Manuscript received September 2, 2020; revised November 8, 2020; accepted December 7, 2020. This work was supported by Defense Research and Development Canada (DRDC), Ottawa, ON, Canada. *(Corresponding author: Symon K. Podilchak.)*

Maksim V. Kuznetcov and Symon K. Podilchak are with the Institute of Digital Communications, The University of Edinburgh, Edinburgh EH9 3JW, U.K. (e-mail: s.podilchak@ed.ac.uk).

Jonathan C. Johnstone and Yahia M. M. Antar are with The Royal Military College of Canada, Kingston, ON K7K 7B4, Canada (e-mail: antar-y@rmc.ca).

Michel Clénet is with the Defense Research and Development Canada, DRDC, Ottawa, ON K1N 1J8, Canada (e-mail: michel.clenet@drdc-rddc.gc.ca).

Color versions of one or more figures in this article are available at https://doi.org/10.1109/TMTT.2021.3053980.

Digital Object Identifier 10.1109/TMTT.2021.3053980

polarization modulation techniques [12]–[14]. In addition, polarization diversity also opens new possibilities in these microwave systems, such as improved network reliability and reduced power consumption [15], [16].

One such structure with polarization diversity and with dual-port excitation is the cross-shaped DR proposed in [17]. This antenna demonstrated CP polarization with a bandwidth of 6.8% and LP radiation over a bandwidth of 38.5%. The antenna exploits the quasi-TM_{111} and the TE_{111} modes by driving its two different ports. That work also examined the limitation of the feeding system (such as its asymmetry), which can cause mode degradation and the related nonstable radiation pattern for the CP polarization state. This C-band antenna can be used in satellite systems or other commercial transponder systems. Another way to achieve polarization control is to introduce p-i-n-diodes and tunable feeding networks. For example, the DR and circuit system (DRCS) in [18] was realized by a coupler type feeding system with eight p-i-n-diode switches, which established phase shifts between the output ports of the coupler. This offered reconfigurability, i.e., right-handed circular polarization (RHCP), left-handed circular polarization (LHCP), and orthogonal LP polarization states with maximum bandwidths of 6.3% and 9.5%, respectively. This S-band antenna [18] can be used in commercial Wi-Fi applications, satellite communications, or other robust systems, which utilizes polarization agility.

Given those findings, investigations to simplify the overall design of DRCSs while reducing feeding network size have attracted our interest. For example, previous work by some of the authors in [19] considered an eight-port DR structure for polarization diversity applications by the generation of LHCP, RHCP, and LP. Such an antenna system required a network of external couplers and an eight-port feeding configuration. To advance this design, a similar antenna system (but with only four-ports) was made more efficient and compact in [20] by using a meandered slot ring with a metallic cavity backing. In particular, the DR element was reduced in size by using a high relative dielectric constant material, and similar to [19], CP radiation over a wide frequency band (35%) was achieved only for the four-port antenna by using external couplers.

Most of the feeding systems for polarization control or reconfigurability can be divided into active or passive circuit solutions. An example of such a passive system was presented in [21], where a dually polarized waveguide coupler system was presented, which operated at 60 GHz. The proposed feeding system enabled an efficient power split ratio that can be useful in base station applications. Also, in that work, a dual-polarized Butler matrix feeding system was adopted, verifying the capabilities of the beam-forming network.

Another reconfigurable system was presented in [22]. The described waveguide antenna feeder provided an efficient signal rotation between LHCP and RHCP. Also, by utilizing piezo-motors integrated within the waveguide system, the authors were able to achieve a compact design while maintaining a high-efficiency power split ratio. The reported polarizer operated from about 13 to 15 GHz with an axial ratio below 3 dB. An example of an active system could be reconfigurable elements based on p-i-n switches. The antenna

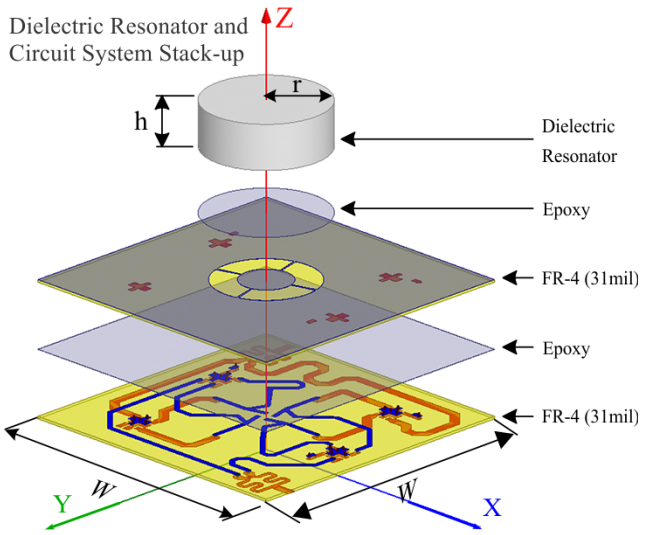

Fig. 1. Complete stack-up for the proposed DRCS defined by two 31-mil FR-4 substrates, two epoxy layers, surface mount components, and the cylindrical DR itself. Dimensions h, W, and r are 18.1, 90, and 19.05 mm, respectively. In terms of size with respect to the wavelength, the total structure is 0.54 λ_0 × 0.54 λ_0 × 0.1 λ_0 (at the higher operational frequency range, which is about 1.8 GHz).

design presented in [23] utilized such a diode system to control beam properties of the dipole antenna array. This structure operated from about 24 to 27.5 GHz with a maximum realized gain of 10 dBi and 90% efficiency. The antenna was also integrated within a mobile phone model, suggesting that such a structure could be applicable for 5G communication systems.

Following these developments, we propose in this article a new L-band DRCS, i.e., a DRCS, with only two external ports, which offers RHCP, LHCP, and two orthogonal LP operating states (see Figs. 1–3). As a starting point in our design, the preliminary efforts in [24] for the simulated eight-port DRA were reviewed and studied. Expanding on these findings, a totally new feeding system was designed and fully integrated under the DR ground plane (see Fig. 1). Then, this DRCS was fabricated and experimentally verified to demonstrate polarization agility. The particular choice of the L-band frequency range, while offering polarization diversity, can support connectivity to the Global Navigation Satellite System (GNSS), the Global Positioning System (GPS), and other wireless communication systems where polarization diversity and polarization purity are of interest [25]. Using this antenna diversity and the supporting signal processing techniques, as outlined in [26] and [27], noise effects can be reduced and channel fading mitigated.

The antenna circuit system (CS) reported in this article, for operation in the L-band, offers similar compactness to [20] but also with the noted integrated feeding [see Fig. 2(b)]. In addition and as further discussed in this article, a more complicated DR excitation approach enabling polarization diversity is employed. With such compactness into a single antenna unit, there are many benefits when adopting such a DRCS for real-life scenarios. However, as further outlined herein, there are also some minor design constraints. This includes acceptable coupling within the circuit and reduced

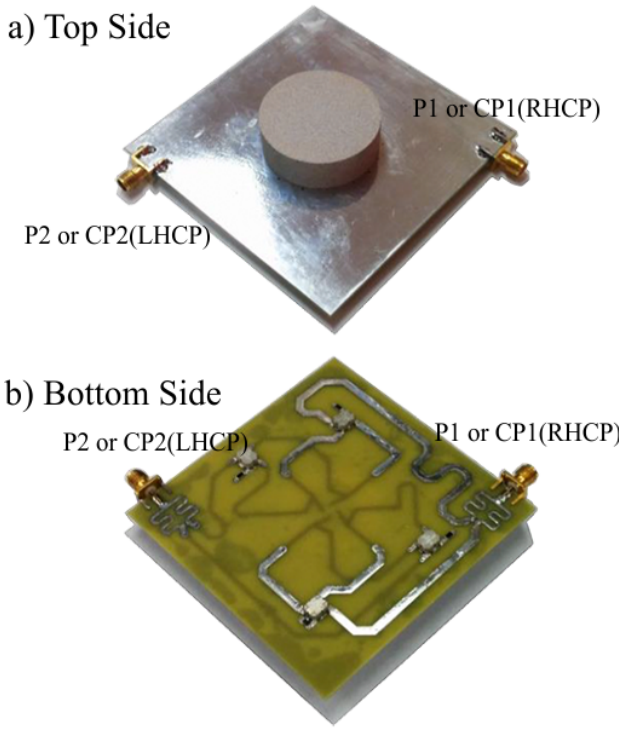

Fig. 2. (a) Top view and (b) bottom view for the fabricated DRCS (total dimensions: 90 × 90 × 19.7 mm^3, excluding connectors); see the multilayer stack-up for the relevant circuit and ground plane layers, as shown in Fig. 1.

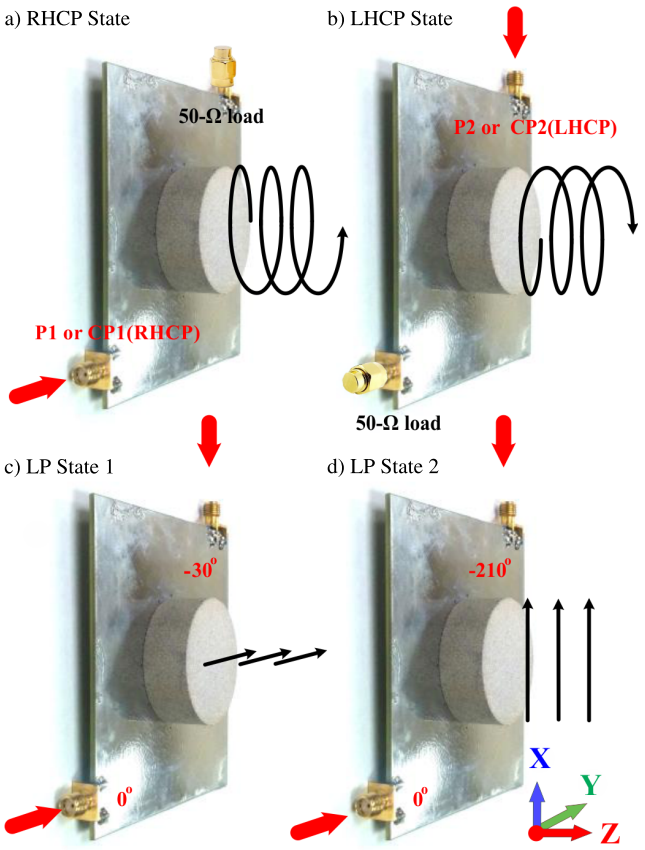

Fig. 3. Illustration of the possible polarization states for the two-port DRCS where the relevant ports are driven and the nonactive ports are terminated with 50-Ω loads: (a) RHCP, (b) LHCP, (c) LP state 1 (dominant in the y–z plane), and (d) LP state 2 (dominant in the x–z plane).

DRCS total efficiency, the need for an external combiner and phase shifter for LP operation, and reduced realized antenna gains when using commercially printed circuit board (PCB) dielectric materials of low cost, i.e., FR-4. As further discussed in this article, solutions include redesigning the feeding network, to better support LP operation, at the cost of an enlarged circuit layout size and using lower-loss PCB substrates to enhance DRCS efficiency.

Regardless of these points, the fabricated and measured DRCS reported for proof-of-concept is well matched between 1.25 and 1.9 GHz, defining the −10 dB impedance reflection coefficient bandwidth (which is in excess of 40%). Also, the simulated total DRCS efficiency (antenna and feeding system) for all polarization states is about 70% or more. Measured beam patterns are documented, as well as the realized gain over the frequency with results in agreement with full-wave simulations. Simulated and measured axial ratios for the LHCP and RHCP states are also well below 3 dB over the DRCS operational frequency range. To the best of our knowledge, no similar antenna structure with an integrated feeding system has been reported offering comparable functionality in terms of overall compactness, broadband operation, and polarization diversity.

II. DRCS Design

As an initial step in the design and development of the proposed DRCS, the cylindrical DR with the basic feeding system from [24] is reviewed. That preliminary feeding system was defined by a network of eight microstrip lines etched on the bottom side of the substrate to feed four aperture coupled slots (ACSs) that were positioned on the bottom side of the DR (see inset of the eight-port feeding system in Fig. 4). This eight-port structure was able to provide a high degree of freedom, and when applying the appropriate (and fixed) phase shifts to the ports (see Table I), the excitation and control of degenerate $HE_{11\delta}$ modes were made possible. As a result, an agile eight-port polarization diverse antenna [24] was simulated and optimized, which offered LP, LHCP, and RHCP radiation.

The realized gains in the far-field for the polarization states described in Table I can also be plotted versus frequency, as shown in Fig. 4, considering a relative dielectric constant (ϵ_r) of 27 for the DR. While polarization diversity can be observed for the eight-port DRA (see Fig. 4), and some preliminary simulations were reported in [24] with $\epsilon_r = 30$ for the DR (while both adopting ideal port excitation), no practical feeding circuit was developed. As further described herein, a new feeding system with only two external ports is designed for complete DRCS integration, allowing for dual-CP and dual-LP operations.

A. General DRCS Structure Overview

The proposed DRCS consists of an optimized cylindrical DR ($\epsilon_r = 27$) having a radius of 19.05 mm and a height of 13.80 mm (see Figs. 1–3). This DR and its ground plane are placed on top of two 31-mil square FR-4 substrates, each

TABLE I
FEED DEFINITIONS FOR THE POLARIZATION STATES (SEE FIG. 4)

Port	RHCP	LHCP	LP (Horizontal)	LP (Vertical)
P1	$1\angle 0°$	0	$1\angle -30°$	$1\angle -210°$
P2	$1\angle 270°$	0	$1\angle 240°$	$1\angle 60°$
P3	$1\angle 180°$	0	$1\angle 150°$	$1\angle -30°$
P4	$1\angle 90°$	0	$1\angle 60°$	$1\angle -120°$
P5	0	$1\angle 0°$	$1\angle 180°$	$1\angle 210°$
P6	0	$1\angle 90°$	$1\angle 270°$	$1\angle 300°$
P7	0	$1\angle 180°$	$1\angle 0°$	$1\angle 30°$
P8	0	$1\angle 270°$	$1\angle 90°$	$1\angle 120°$

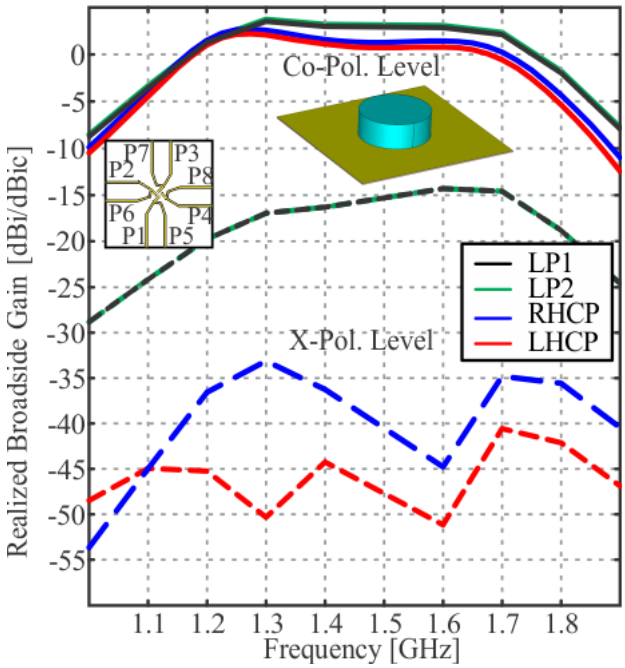

Fig. 4. Simulated gain and cross-polarization levels for a representative eight-port DR structure (see inset for the bottom view and top view) while considering the (ideal) port definitions, as outlined in Table I from 1 to 2 GHz. Note that no feeding circuit, as shown in Fig. 2(b), was included in the simulation model.

having dimensions of 90 mm × 90 mm. The four radiating $HE_{11\delta}$ modes of the DR are excited by four radial ACSs. The slots are driven by the aforementioned feeding circuit (see Fig. 5), which shares the ground plane of the top cylindrical DR element. Basically, each port of the DRCS when driven generates either RHCP or LHCP. These external ports define the input connections to two distinct planar circuits, and given the compact implementation, these circuits become colocated.

As outlined in Figs. 1 and 2, these RHCP and LHCP feeding circuits are realized by a bottom microstrip transmission line layer and an inner strip layer (or buried microstrip). This ensures overall structure compactness and full integration with the top DR element. In addition, for some practical applications and when interference from other radiation sources can be problematic, the bottom side of the DRCS can be covered with a metal sheet, or the feeding system can be placed inside a cavity, as in [20]. Full-wave simulations suggest that an air gap of at least 6 mm between the bottom PCB (of the DRCS) and any additional metal sheeting for shielding purposes is required. This can help to minimize any unwanted coupling

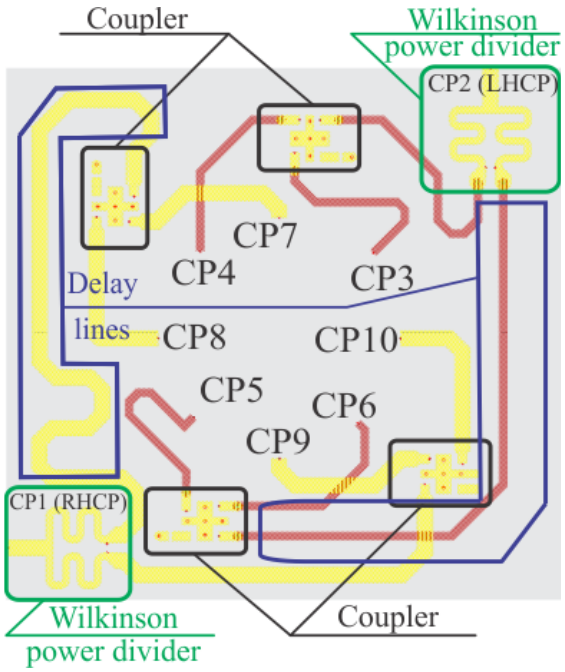

Fig. 5. Intermediate layout of the feeding network for design and simulation purposes; for the final PCB circuit dimensions, see Fig. 10 and Table II, respectively. As outlined in Fig. 1, the feed circuit is composed of two FR-4 dielectric layers having a common ground plane and ten circuit ports, i.e., CPi, where $i \in [1, 10]$. Microstrip transmission lines (yellow trace) are attached to the two external ports (i.e., P1 or CP1 and P2 or CP2; see Fig. 2), while the inner strip transmission lines or buried microstrip (red trace) are connected to the eight internal ports for DR feeding: CP3, CP4, CP5, CP6, CP7, CP8, CP9, and CP10. It should be mentioned that the microstrip and strip lines were electrically connected by metalized vias, while ideal magnitude and phase responses were defined for the four surface mount couplers during simulations.

effects and detuning of the microstrip line-based feed system (all results not reported for brevity).

It can be noted that the realized gain traces in Fig. 4 consist of two peaks: one located at about 1.25 GHz and the other at 1.65 GHz. The 1.25-GHz peak is related to the resonances of the ACSs that are driven by the feeding circuit. These slots also transfer power to the DR for hybridized radiation into the far-field. The 1.65-GHz peak can be attributed to strong $HE_{11\delta}$ mode excitation. It is the combination of these two complementary radiation mechanisms, which supports the broadband DRCS performance, while it is the high relative dielectric constant material for the resonator and its PCB feeding circuit, which dictates overall DRCS compactness.

B. Design and Operation of the Feed Circuit

The antenna feeding circuit layout overview for overall DRCS design purposes can be seen in Fig. 5, and the motivation for this structure was primarily to achieve CP operation by either a sequential $+90°$ or $-90°$ applied to the four ACSs. However, LP operation can be made possible using external phase shifters and will also be described herein.

1) Circularly Polarized Radiation: To achieve LHCP for example, a $+90°$ sequential phase shift is achieved by taking power incident on a single port (see Figs. 2 and 3) and then having it divided through a meandered and compact Wilkinson power divider in order to achieve a 3-dB power split. Each

of these two split signals is then routed to a 90° surface mount hybrid coupler (Anaren model XC1400P-03S), which further splits the input power while also adding a 90° delay. This results in four signal paths, i.e., two signals in phase and two signals with a 90° relative phase shift. However, sequential +90° is required at the ACSs for LHCP operation, i.e., 0°, +90°, +180°, and +270°. These last two phase shifts are obtained by passing one of the two signal lines from the Wilkinson power divider through a 180° long trace or delay line (designed with a 1.3-GHz center frequency) prior to another 90° hybrid coupler. Similarly, a sequential −90° phase shift (i.e., 0°, −90°, −180°, and −270°) for RHCP is achieved by a separate and colocated circuit enabling this opposite polarization state. The primary differences being that auxiliary ports on the hybrid couplers are connected to the traces from the power divider.

2) Linearly Polarized Radiation: It is achieved by employing an external power divider and simultaneous excitation of both the LHCP and RHCP ports. However, an external phase shifter providing an offset of either −210° or −30° should be connected to P2 (LHCP) in order to account for path length differences between the two feeding circuits. The two options (−210° or −30°) will provide orthogonal orientations of the radiated fields (see Fig. 3), defining LP state 1 and LP state 2 for the DRCS, respectively.

It should be mentioned that other phase offsets are possible such as 0° and 180° (or 90° and −90°); however, full-wave simulations for the DRCS suggest that −210° and −30° offered increased realized gain values in the far-field. These phase requirements are related to the asymmetry within the feeding circuit, unwanted phase offsets incurred due to electromagnetic coupling within the PCB and transmission line meandering. This transmission line meandering was needed to ensure a compact feeding circuit implementation.

C. Feeding of the Radial ACSs

By inspection of the feeding circuit and the slots positioned under the DR element (see Figs. 1 and 2), it can be observed that two transmission lines that originate from the hybrid couplers drive each of the four ACSs, for example, CP3 and CP7 or CP4 and CP8. The radial positioning of these slots, and the resulting physical connection of the lines, was required due to the high relative dielectric constant of the DR ($\epsilon_r = 27$), which enabled overall structure compactness. This resulted in an eight-point feed arrangement for the cylindrical DR element. It should also be mentioned that, while considering these design constraints, a parametric optimization for the relevant dimensions of the DR (such as radius and height of the DR, as well as the radius, orientation, and position of the ACSs, while excluding and then including the feeding circuit) was completed using a commercial full-wave simulator. Results suggest that the best possible matching was achieved from about 1.1 to 1.7 GHz with maximum realized gain values, as reported in Fig. 4, for the case without the integrated feeding circuit.

It should be mentioned that coupling is not significantly increased with these physical connections of the transmission lines near the ACSs [see Figs. 1 and 2(b)] compared to more classic open-circuited stub matching techniques, as adopted in [19]. This is because the majority of any coupling is mainly generated by the adjacently positioned strip lines, which feeds the common slots and not the connected stubs positioned near the origin. In fact, it was found, that during our design work, the connected transmission lines under the DR provide some reactive loading and can be utilized when matching and improving power delivery to the slots for hybridized radiation of the ACSs with the DR.

III. Feed Circuit and DRCS Simulations

To further design the feeding network, the PCB circuit in Fig. 5 was optimized using a commercial circuit simulator, in particular, dimensions of the Wilkinson power dividers, the placement of the via interconnections, and the equal phase delay lines positioned between couplers and other connection points. There are also two 180° delay transmission line (see Fig. 4), considering a center frequency of 1.3 GHz to achieve the required phase delays (see Table I) at the feed points of the DR element. In addition, similar circuit performances were also desired from about 1.1–1.7 GHz. The simulations were initially completed having no DR element placed on top of the structure while using the circuit, as illustrated in Fig. 5.

The feed system was also carefully designed and optimized by considering the possible electromagnetic coupling effects between transmission lines and any unwanted phase offsets accrued due to meandering. In particular, traces were separated as much as possible, while corner chamfers, due to the meanders and 90° bends, were taken into consideration during the DRCS optimization. This ensures phase stability and improves the overall response of the circuit system. In the following, simulation results for the various circuit parts are reported realizing the various polarization states and the generated electric field within the PCB for the RHCP state (see Figs. 6–9). Detailed dimensional layouts for the final and fabricated feeding circuit are outlined in Fig. 10 and Table II. Simulated losses, phase imbalances, and total DRCS efficiency values are also reported in Figs. 11 and 12 and Table III.

A. Excitation of DRCS Port 1 or CP1 for RHCP

The first external port, CP1, divides the input signal to circuit ports CP7, CP8, CP9, and CP10 for RHCP. The feeding network magnitude and phase imbalances can be seen in Fig. 6. It should be noted that the magnitude imbalance is no more than 0.8 dB across the entire simulated range, from 1 to 2 GHz, which is slightly higher than the magnitude imbalance for the LHCP feeding circuit (see Fig. 8).

The different electrical lengths for the transmission lines connected to CP7 and CP8 as well as CP9 and CP10 provide the required phase at 1.3 GHz as per design (see Fig. 6). For example, it can be seen that a sequential 90° phase shift is achieved at that frequency (as required with reference to Table I for the RHCP state). For other frequencies, the electrical lengths of the microstrip lines are naturally different due to dispersion, and it can be observed that, at 1.1 and 1.5 GHz, the required sequential phase difference is offset by about 25°

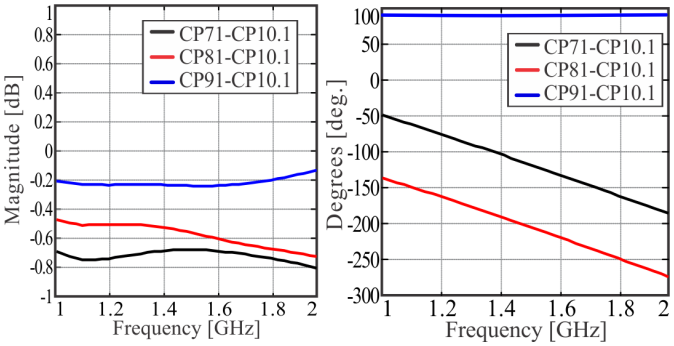

Fig. 6. Simulated response of the feeding network for the RHCP state without the DR (see Fig. 5). The maximum magnitude imbalance is approximately 0.7 dB at the 1.3-GHz circuit center frequency, which is slightly higher when compared to the LHCP state (see Fig. 8). Phase differences are ±90° or −180° at 1.3 GHz, which is similar to the LHCP state.

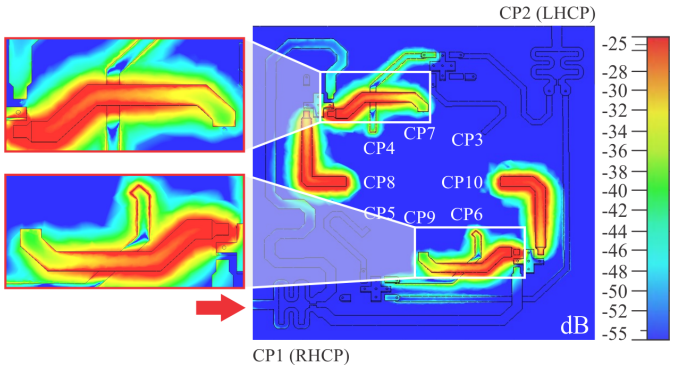

Fig. 7. Simulated E-field at 1.3 GHz within the central part of the feeding circuit (bottom view) for the RCHP state and where power is injected into P1 or CP1. Due to the compactness of the structure, the microstrip and strip lines crossover in particular sections. This allows for unwanted (minor) cross-coupling between the two main CP circuits (see insets), and this can be observed between the transmission lines connected to internal ports CP4 and CP7, and CP6 and CP9 (whose S-parameter coupling values are below −20 dB). Similar observations were made for the LHCP and LP states (all results not reported for brevity).

(see Fig. 6). Similar phase responses are observed for the LHCP circuit part.

The observed minor magnitude and phase imbalances in Fig. 6, which are unwanted and can detune DRCS operation, are related to the signal crosstalk between the colocated LHCP and RHCP feed circuits. A full-wave simulation of the electric field within the PCB for this polarization state confirms that unavoidable electromagnetic coupling occurs at the crossover sections of the microstrip and strip lines near CP4 and CP7, as well as CP6 and CP9 (see insets in Fig. 7). The simulated cross-coupled power from 1 to 2 GHz showed values below −20 dB for both cases. It should be mentioned that the full-wave simulator did account for this coupling during the feeding circuit optimization, i.e., the refinement of the detailed metallic patterning features, such as the transmission line bends and meandering (see Fig. 10 and Table II). However, this unavoidable coupling within the colocated RHCP and LHCP circuit parts can still moderately detune circuit performance for the different external port excitations (which enables the various polarization states) contributing to the observed magnitude and phase imbalances reported in Fig. 6.

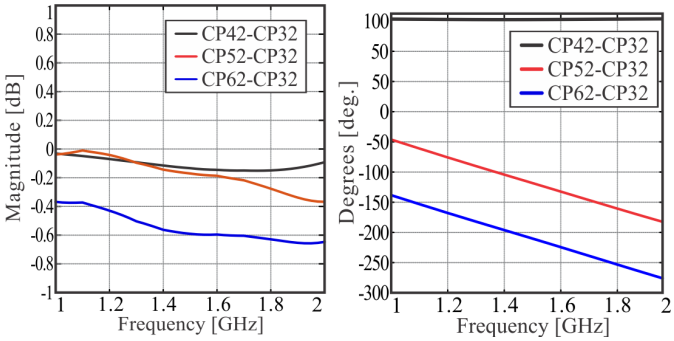

Fig. 8. Simulated response of the feeding network for the LHCP state without the DR (see Fig. 5). The magnitude imbalance is about 0.6 dB for 1.7 GHz (or below), while the general phase response is similar to the RHCP case (see Fig. 6) but with a reverse sequential phase rotation.

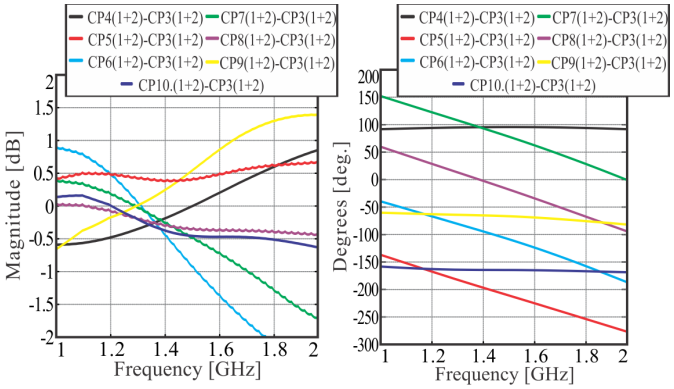

Fig. 9. Simulated response of the feeding network for the LP1 state without the DR considering the circuit in Fig. 5. It is important to note that due to the asymmetry of the design and its compactness, the phase response needs to be corrected so that the phase shifts, as described in Table I, are achieved at the internal ports. Basically, in this simulation, an ideal phase shift of −30° was defined (to represent any external mechanical phase shifter). It is important to note that the magnitude imbalances are ±0.5 dB at about 1.35 GHz, while phase differences are near 0, ±90°, or ±180°.

By inspection of Fig. 7, it can be observed that such coupled power would be absorbed in the resistive loads connected to the hybrid couplers decreasing efficiency. These E-field simulations for the RHCP state in Fig. 7 are very similar to the LHCP case and are not reported for brevity. Regardless of these points, the losses for the RHCP circuit part are less than 1 dB at the circuit design frequency of 1.3 GHz when considering no losses for the PCB and tan $\delta = 0.02$, as reported in Fig. 11. Efficiency values for the complete DRCS range from 74% to 83% when all PCB loss cases are compared (see Fig. 12 and Table III) while considering common conductor losses associated with the copper traces and the ground plane.

B. Excitation of DRCS Port 2 or CP2 for LHCP

When circuit port 2 (CP2) of the DRCS is driven, LHCP radiation can be made possible. Basically, the input signal is mostly divided equally to circuit ports CP3, CP4, CP5, and CP6 and, ideally, with the phase delays, as outlined in Table I. Also, for this state, simulations suggest that the imbalance of those ports can reach maximum values that are less than 0.5 dB at 1.3 GHz (see Fig. 8). Close to ideal phase imbalances can also be observed at 1.3 GHz. This is related to the optimized

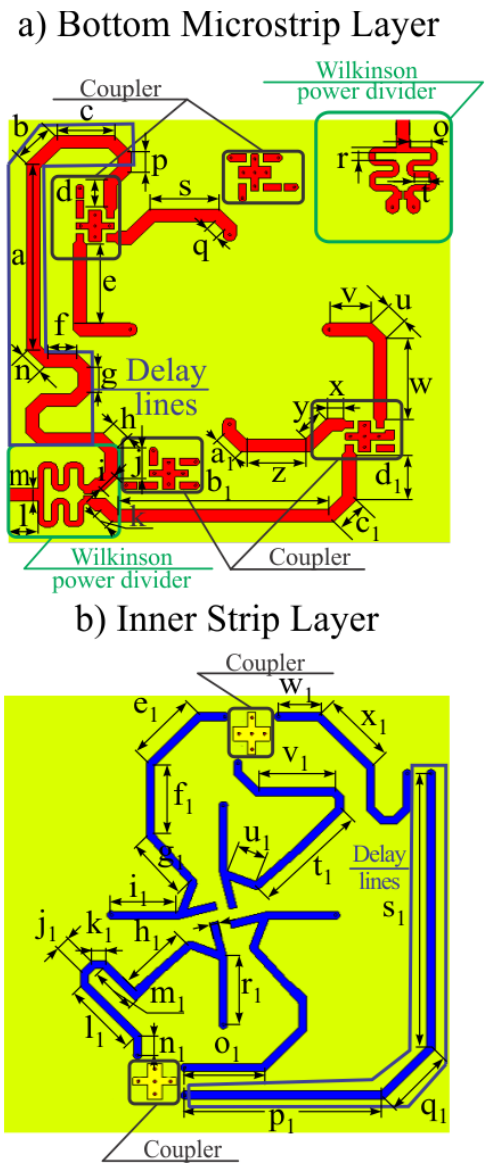

Fig. 10. Final layout of the feeding circuit (relevant dimensions in Table II). (a) Bottom 31-mil-thick FR-4 layer and where the top-face of the microstrip lines are shown. (b) Middle strip trace layer. This layout defines the inner layer which employs microstrip covered by 31-mil-thick FR-4, i.e., a strip layer.

electrical lengths of the transmission lines connected to CP3, CP4, CP5, and CP6.

The overall circuit losses for this LHCP state are compared to other states (see Fig. 11) considering a lossless and lossy FR-4 feeding circuit structure. Maximum efficiency for the LHCP state can be seen at 1.35 GHz with a value of 73%. Simulations in Table III also report different values of $\tan\delta$ for the two FR-4 PCB layers (no loss with $\tan\delta = 0$, low-loss, i.e., where $\tan\delta = 0.002$ representing a hypothetical dielectric PCB material, and standard FR-4 with $\tan\delta = 0.02$). It can be observed that when comparing the maximum feed circuit imbalances for different values of $\tan\delta$, the total DRCS efficiency increases (see Fig. 12) for lower dielectric losses. This makes sense since the signal along the circuit path accrues higher losses (for larger values of $\tan\delta$) that dictate a larger magnitude imbalance for the entire feeding circuit.

TABLE II

DRCS FEEDING CIRCUIT DIMENSIONS AS ILLUSTRATED IN FIG. 10 (ALL VALUES IN MILLIMETERS)

a	**b**	**c**	**d**	**e**	**f**	**g**	**h**	**i**
39.5	8.2	11.8	5.8	16.7	5.5	5.1	4.3	4
j	**k**	**l**	**m**	**n**	**o**	**p**	**q**	**r**
6.2	2	6.2	2.7	5	3.9	4.0	2.6	1.4
s	**t**	**u**	**v**	**w**	**x**	**y**	**z**	$\mathbf{a}_1$
14	2.8	4.2	8.6	17	3.1	6.2	12	4.9
$\mathbf{b}_1$	$\mathbf{c}_1$	$\mathbf{d}_1$	$\mathbf{e}_1$	$\mathbf{f}_1$	$\mathbf{g}_1$	$\mathbf{h}_1$	$\mathbf{i}_1$	$\mathbf{j}_1$
42.6	9.7	9.7	12.9	12.4	12.9	12.7	11.6	2.8
$\mathbf{k}_1$	$\mathbf{l}_1$	$\mathbf{m}_1$	$\mathbf{n}_1$	$\mathbf{o}_1$	$\mathbf{p}_1$	$\mathbf{q}_1$	$\mathbf{r}_1$	$\mathbf{s}_1$
2.6	13.4	8.3	3.5	14.2	35	12.7	11.7	50.3
$\mathbf{t}_1$	$\mathbf{u}_1$	$\mathbf{v}_1$	$\mathbf{w}_1$	$\mathbf{x}_1$				
20.7	5.4	13.5	7.3	13.7				

For example, for $\tan\delta = 0$ [$\tan\delta = 0.02$], the maximum simulated circuit imbalances are 0.50 dB [0.62 dB], while the total peak DRCS efficiency is 80% [68%] for the LHCP state.

It is also important to note that the circuit and DRCS efficiency is generally improved for the RHCP state compared to the LHCP state. This is related to the fact that the majority of the RHCP circuit part is defined by a conventional microstrip transmission line [see the red trace in Fig. 10(a)] with the signal path defined by an air-dielectric medium versus the strip lines (or the microstrip immersed in dielectric) for the LHCP circuit part [see the blue trace in Fig. 10(b)]. Basically, the LHCP circuit part accrues more dielectric and conductor losses for this compact circuit configuration.

C. Simultaneous Excitation of DRCS Ports 1 *and* 2 *for LP*

In this state, both DRCS ports are activated (RCHP port and LHCP port). However, to obtain the required phases for the two LP states, as defined in Fig. 3 and Table I, external phase shifters and power combiners are required. To simulate the circuit response, ideal phase shifts of $-30°$ for LP1 and $-210°$ for LP2 were considered in the simulation model from 1 to 2 GHz and by assigning the required port definitions. For brevity, only the results for the $-30°$ case are reported in Fig. 9, i.e., the LP1 state, as similar results were observed for the LP2 state.

For both LP states, the magnitude imbalance is less than 0.5 dB at 1.3 GHz, while the phases are offset by about 20° or less, and this is related to the aforementioned coupling between the LHCP and RHCP circuit parts. However, the overall DRCS performance is acceptable for the LP states (see Figs. 11 and 12 and Table III) and the optimized circuit parts, as shown in Fig. 10, which achieved the required wideband performance within the commercial simulator. Moreover, it was not possible to achieve the required phase for all the possible polarization states and over the frequency range from 1.1 to 1.7 GHz. From these studies, it is likely that the LP states will have more narrowband performance compared to the LHCP or RHCP states in practice, mainly because the noted phase offsets of $-30°$ for LP1 and $-210°$ for LP2 can be difficult to achieve with an external phase shifter and power divider combination, while also, over the required frequency range to enable broadband LP operation.

TABLE III
SIMULATED PCB FEEDING CIRCUIT PERFORMANCE AND DRCS EFFICIENCY (SEE FIG. 12) CONSIDERING DIFFERENT VALUES FOR tan δ

	RHCP State		LHCP State		LP States	
PCB tan δ	Maximum Feed Circuit Imbalance	Peak DRCS Efficiency	Maximum Feed Circuit Imbalance	Peak DRCS Efficiency	Maximum Feed Circuit Imbalance	Peak DRCS Efficiency
0.000 (ideal)	0.48 dB	83 %	0.50 dB	80 %	1.10 dB	81 %
0.002	0.52 dB	82 %	0.51 dB	79 %	1.50 dB	80 %
0.020 (FR-4)	0.78 dB	74 %	0.62 dB	68 %	2.00 dB	72 %

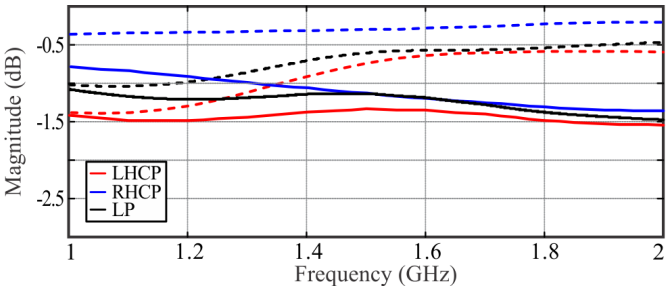

Fig. 11. Simulated losses for the feeding network without the DR element (see Fig. 5). Dashed lines considers no PCB dielectric losses, i.e., tan $\delta = 0$, while the solid lines defines the employed FR-4 material (tan $\delta = 0.02$). It can be observed that the LHCP circuit part has increased losses compared to both the RHCP and LP states. Note that both LP states offer consistent losses.

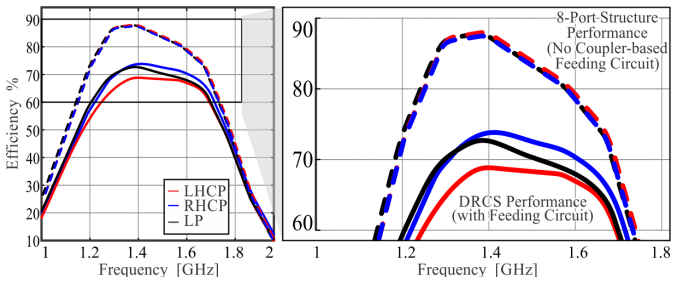

Fig. 12. Simulated efficiency for the DRCS without (see Fig. 4) and with the feeding circuit system. Values are 65% or more from 1.25 to 1.70 GHz considering the employed FR-4 substrate defined by tan $\delta = 0.02$. Improved efficiency is possible with PCB substrates having reduced dielectric losses (see Table III).

The simulated losses for these LP states are about the mean for the RHCP and the LHCP states (see Fig. 11 and Table III). For example, the simulated efficiency of the DRCS considering LP operation is slightly lower than the RHCP state with values ranging from 72% to 81% for the various PCB loss cases, as outlined in Table III. Regardless of these results, simulations suggest that the LP states can be made possible.

D. DRCS Structure Considerations and Simulations

It should be noted that the DRCS was originally designed considering $\epsilon_r = 30$ for the DR element, as in [24]. However, after further experimental study and by following [20], the relative dielectric for the DR was defined as 27 for the full-wave simulations (in Figs. 4 and 12), rather than 30, the nominal value reported by the manufacturer on the material data sheet. This is related to the given rated variance specification for the dielectric material, $\varepsilon_r = 30 \pm 10\%$ (Eccostock HiK500F). Given these findings, all simulation results provided in this article are those for a DR with $\epsilon_r = 27$ and not 30, providing a valid comparison with any measurements.

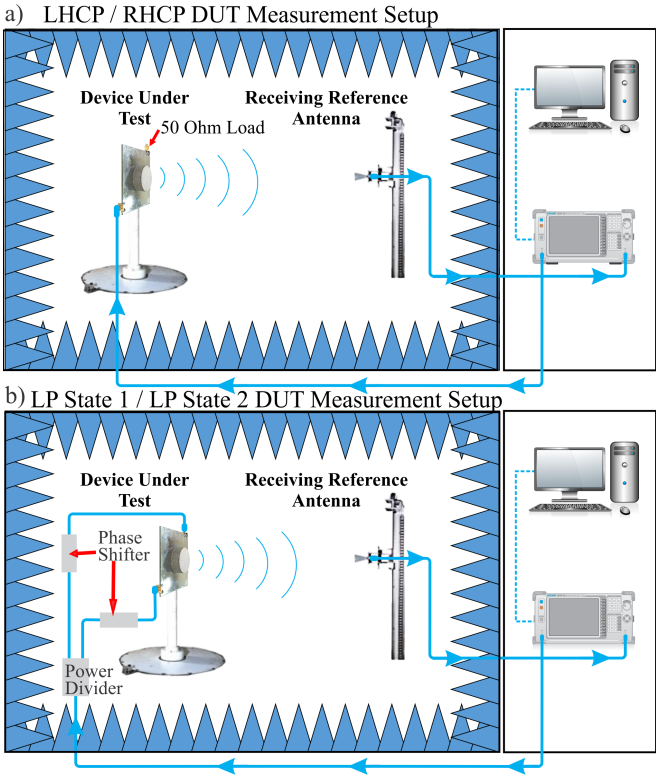

Fig. 13. Far-field measurement setup: (a) one-port configuration for CP and (b) two-port for LP. For the CP states, one of the ports was terminated with a 50-Ω load, as shown in Fig. 3. An external power divider and mechanical phase shifters were used to excite both ports for the LP states (see Fig. 3). It should be highlighted that two equivalent phase shifters were employed in the LP measurements and that the relative phase differences were defined as required, i.e., $-30°$ and $-210°$ for LP state 1 and LP state 2, respectively.

IV. RESULTS AND DISCUSSION

The proposed DRCS (see Figs. 1 and 2) was fabricated and then measured using the anechoic chamber facilities at The Royal Military College of Canada. The DRCS measurement setup can be better understood in Fig. 13, while a photograph of this device under test (DUT) positioned within the anechoic chamber can be observed in Fig. 14. The DRCS was measured in transmit mode where the reference horn antenna was used as the receiver (see Fig. 13). As discussed previously, to measure the DRCS response when considering CP operation, one of the ports was terminated with a 50-Ω load (see Fig. 3). For both LP cases, external phase shifters (mechanical) were employed, as well as a power divider. The resulting far-field beam patterns, realized gains, axial ratios, and port matching values are reported in Figs. 15–19.

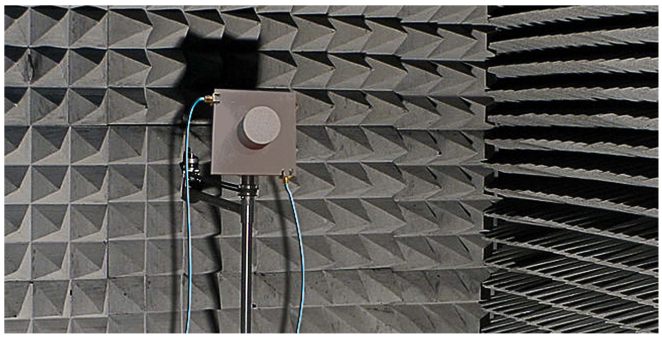

Fig. 14. Photograph of the DUT for far-field characterization: DRCS defined by a top cylindrical DR element and its integrated PCB feed circuit.

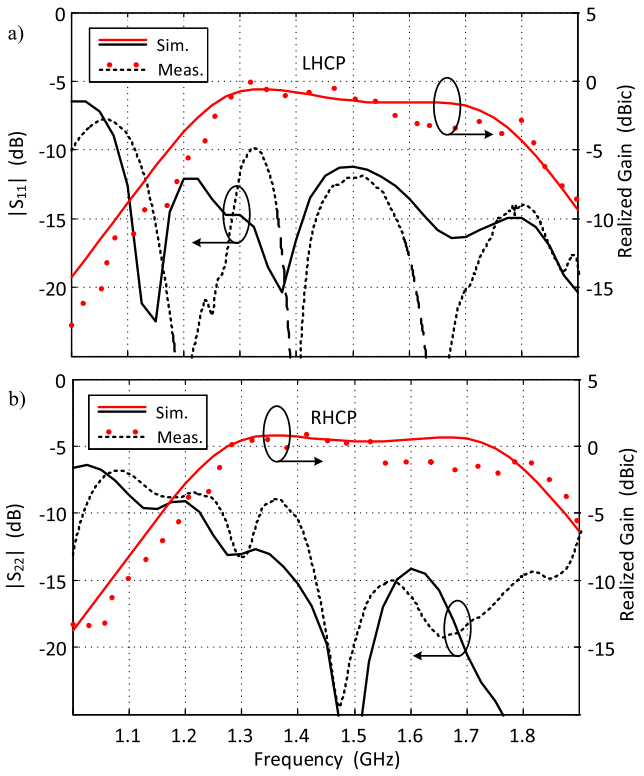

Fig. 15. (a) Simulated and measured LHCP gain and reflection coefficient. (b) Simulated (solid) and measured (dashed/dotted) reflection coefficient and realized RHCP gain at broadside versus frequency.

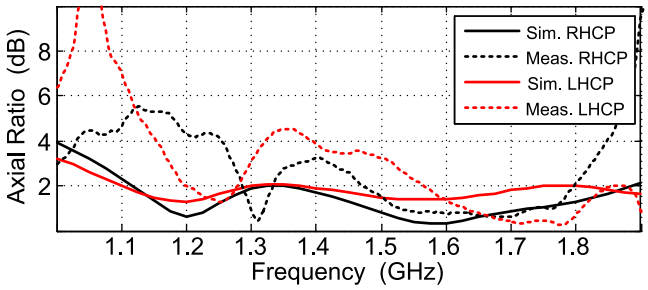

Fig. 16. Simulated (solid) and measured (dashed) axial ratios at broadside for the LHCP (red) and RHCP (black) states compared to the frequency.

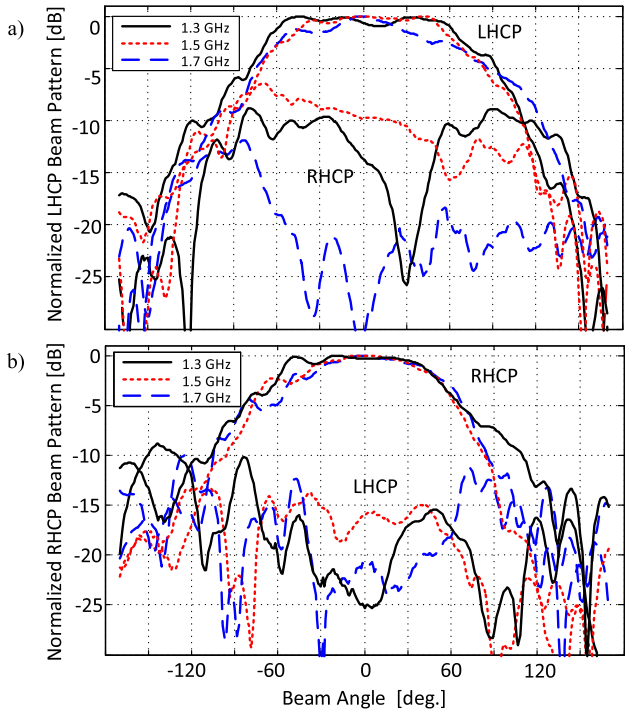

Fig. 17. Measured (a) LHCP and (b) RHCP beam patterns in the $\phi = 0°$ plane. Normalized patterns are shown at 1.3, 1.5, and 1.7 GHz (similar patterns were observed over the operating band of the DRCS).

Referring to Fig. 15(a), the LHCP port of the DRCS has a measured −10-dB reflection coefficient bandwidth from 1.11 to above 1.90 GHz. The peak gain is 0.0 dBic with a 3-dB bandwidth from 1.25 to 1.62 GHz. On the other hand, it can be observed that the RHCP port of the measured DRCS was matched with a −10-dB impedance reflection coefficient bandwidth of 41% from 1.25 to 1.90 GHz (although $|S_{22}|$ does rise above −10 dB slightly at 1.35 GHz). In addition, the peak gain of the DRCS is 1.20 dBic occurring at 1.35 GHz, with a 3-dB bandwidth from 1.25 to 1.83 GHz. The reduced realized gain for the LHCP state is expected and in line with the full-wave simulations since the DRCS efficiency is less than 70% (see Fig. 12). On the other hand, efficiency values are above 70% from 1.3 to 1.6 GHz for the RHCP state. Improved realized gain values are expected for a PCB substrate with less loss than FR-4 (see Figs. 11 and 12 and Table III).

Referring to the axial ratio results in Fig. 16, simulation results are well below 3 dB over the entire operating band of the DRCS. For the measurements, axial ratio values are about 4 dB or below. This minor discrepancy can be related to some fabrication and assembly tolerances, in which the DR element was likely not perfectly positioned on top of the four ACSs.

The RHCP and LHCP radiation patterns were measured and are reported in Fig. 17. It can be observed that, when excited for RHCP radiation, the DRCS offers a 3 dB beamwidth greater than 120° in the elevation plane and a cross-polarization level of −13 dB (at worst) below the copolarized values at broadside. When excited for LHCP operation, the 3-dB angular beamwidth is similar to the RHCP case.

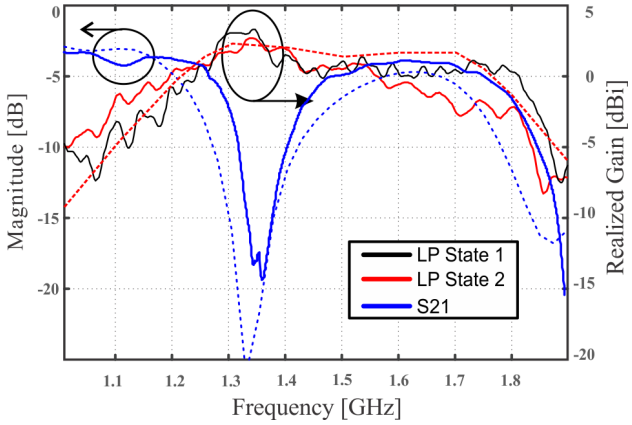

Fig. 18. Measured (solid lines) and simulated (dash lines) coupling and LP gain versus frequency for both states. Calibrated phase offsets defined at 1.35 GHz, which provided the needed −30° and −210° phase offset at the ports, were achieved using a tunable mechanical phase shifter. It can be observed that when the (passive) port coupling $|S_{21}|$ is minimized, the realized LP gain increases.

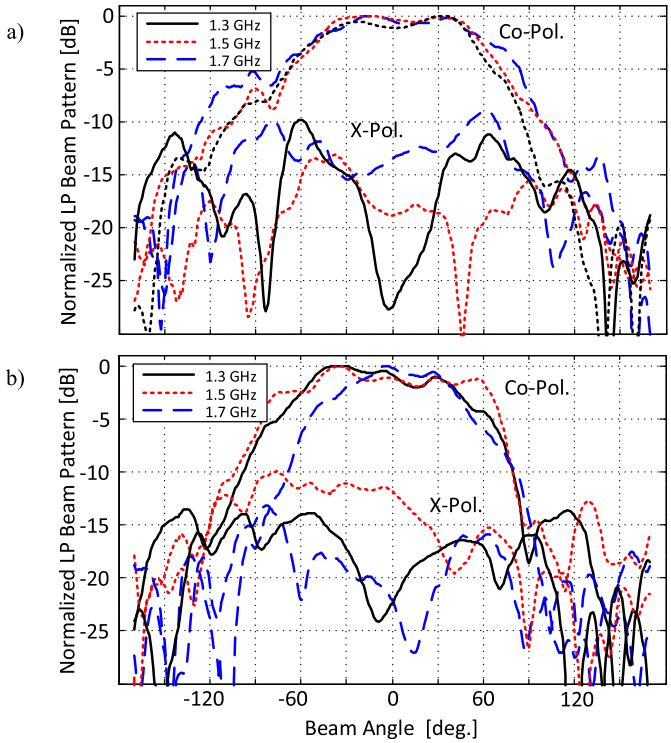

Fig. 19. Measured LP beam patterns generated by excitation of both DRCS ports (see Fig. 3): (a) LP state 1 and (b) LP state 2. Normalized patterns are shown at 1.3, 1.5, and 1.7 GHz. It should be mentioned that the required phase shifts were achieved using a calibrated phase shifter at these three frequencies.

As mentioned previously, in addition to RHCP and LHCP, the two-port DRCS is capable of generating two orthogonal LP states (see Fig. 3). This is achieved through simultaneous excitation of both the RHCP and LHCP ports. Results for these LP states were also measured, and the resulting gain is presented as a function of frequency in Fig. 18, while the normalized beam patterns are reported in Fig. 19.

Comparing Figs. 15 and 18, it can be observed that the LP peak gains are higher than those of both the RHCP and LHCP cases (as also reported in Fig. 4). This is because, during LP operation, the power from both ports is combined [see Fig. 3(c) and (d)], resulting in an overall higher realized gain. Similar results were observed for the full-wave simulations in Fig. 4. In addition, note that the gain profile versus frequency for the studied LP case in Fig. 18 has more variation over frequency than those for the CP cases reported in Fig. 15. This is attributed to several factors, including phase mismatches between the RHCP and the LHCP ports. This was because the required phase offset was provided through an external and tunable phase shifter (which does have some frequency dependence) and unequal amplitudes at the LHCP and RHCP ports (caused by the practically realized and non-symmetric feed system). These factors likely caused different signal amplitudes and minor phase offsets for the two main signal paths.

When considering possible real-life applications for the reported L-band DRCS, such as GNSS/GPS systems, the cross-coupling between the LHCP and RHCP ports is not much of a concern. This is because it can be expected that the same signal will be received at the two ports from the far-field (albeit at different power levels). Also, the polarization of the incoming signal might be elliptical. This would realize an unequal power split ratio onto the antenna, of the same far-field signal, for collection at the external ports. This makes the coupled signal (between ports) of little significance. However, in the case of other RF systems with two different incoming signals onto the antenna and with different polarizations, the circuit coupling within the DRCS should be taken into account. This can possibly be accommodated by introducing some type of filtering within the feed system or by applying some other signal processing techniques. These approaches could help to mitigate any unwanted crosstalk.

Studying the beam patterns in Fig. 19, it can be observed that both LP antenna states have a −3-dB beamwidth of approximately 120°. Furthermore, the cross-polarization levels for the LP states were measured to be (at most) less than 12 dB below the copolarization levels at broadside and as low as −27 dB depending on the observed frequency.

V. Conclusion

In this work, a single DR and feeding circuit system, i.e., a DRCS, were presented. This antenna structure is capable of RHCP, LHCP, and two orthogonal linearly polarized operating states. The two ports of the DRCS were measured to have −10 dB impedance reflection coefficient bandwidths of 41% and 53%, which are representative of the RHCP and LHCP antenna operational states, respectively. In addition, the DRCS was measured and offers peaks gains of 1.2 dBic, 0.0 dBic, 3.6 dBi, and 2.6 dBi for RHCP, LHCP, and both LP orientations, respectively. Furthermore, all CP and LP states were found to have a beamwidth greater than 120° in the elevation plane, and cross-polarization levels are typically in excess of −10 dB.

Improvements that could be made to the DRCS include a modified feeding circuit considering a dielectric substrate with reduced losses compared to FR-4. This would improve DRCS

realized gain values and efficiency. In addition, a modified feeding circuit that includes both the additional transmission line lengths of $-210°$ or $-30°$ could be designed to achieve both, LP, and CP radiation, thus not requiring an external combiner/divider and phase shifter as in the LP case. However, this would require additional delay lines and printed circuit parts, which could increase the physical size of the network and, thus, the entire antenna system. Furthermore, additional feeding circuit losses would be observed due to the added transmission line lengths to achieve such dual-CP and dual-LP operation. To avoid this problem, a dielectric substrate with lower loss could be employed, i.e., not FR-4 as mentioned previously. However, in some cases, only dual-CP operation (and not both dual-CP and dual-LP) might be the main design motivations for the compact DRCS, in which both LHCP and RHCP using two distinct ports are of main interest, as demonstrated in this work.

Overall, this DRCS functionality has been made possible by a compact wideband antenna structure and with a low-cost feeding circuit implementation for dual-CP. External phase shifters were employed to demonstrate dual-LP operation as well and in the main effort to circumvent the aforementioned losses in the compact, and co-located, FR-4 feeding circuit.

REFERENCES

[1] D. Guha, B. Gupta, and Y. M. M. Antar, "Segmented hemispherical DRA: New geometry characterized and investigated in multi-element composite forms for wideband antenna applications," *IEEE Trans. Antennas Propag.*, vol. 60, no. 3, pp. 1605–1610, Mar. 2012.

[2] G. Varshney, V. S. Pandey, R. S. Yaduvanshi, and L. Kumar, "Wide band circularly polarized dielectric resonator antenna with stair-shaped slot excitation," *IEEE Trans. Antennas Propag.*, vol. 65, no. 3, pp. 1380–1383, Mar. 2017.

[3] T. A. Denidni, Z. Weng, and M. Niroo-Jazi, "Z-shaped dielectric resonator antenna for ultrawideband applications," *IEEE Trans. Antennas Propag.*, vol. 58, no. 12, pp. 4059–4062, Dec. 2010.

[4] Y. Gao, Z. Feng, and L. Zhang, "Compact asymmetrical T-shaped dielectric resonator antenna for broadband applications," *IEEE Trans. Antennas Propag.*, vol. 60, no. 3, pp. 1611–1615, Mar. 2012.

[5] B. Bahreini, H. Oraizi, N. Noori, and P. Mousavi, "Optimum design of a beam-forming array of S-shaped DRA elements with a superstrate on an SIW feed for 5G mobile systems," *IEEE Antennas Wireless Propag. Lett.*, vol. 18, no. 7, pp. 1410–1414, Jul. 2019.

[6] M. Yang, Y. Pan, and W. Yang, "A singly fed wideband circularly polarized dielectric resonator antenna," *IEEE Antennas Wireless Propag. Lett.*, vol. 17, no. 8, pp. 1515–1518, Aug. 2018.

[7] R. Dutt Gupta and M. Singh Parihar, "Differentially fed wideband rectangular DRA with high gain using short horn," *IEEE Antennas Wireless Propag. Lett.*, vol. 16, pp. 1804–1807, 2017.

[8] M. S. Sharawi, S. K. Podilchak, M. U. Khan, and Y. M. Antar, "Dual-frequency DRA-based MIMO antenna system for wireless access points," *IET Microw., Antennas Propag.*, vol. 11, no. 8, pp. 1174–1182, 2017.

[9] M. S. Sharawi, S. K. Podilchak, M. T. Hussain, and Y. M. M. Antar, "Dielectric resonator based MIMO antenna system enabling millimetre-wave mobile devices," *IET Microwaves, Antennas Propagation*, vol. 11, no. 2, pp. 287–293, 2017.

[10] R. Yaduvanshi and H. Parthasarathy, *Rectangular Dielectric Resonator Antennas: Theory Design*, Jan. 2015.

[11] S. Keyrouz and D. Caratelli, "Dielectric resonator antennas: Basic concepts, design guidelines, and recent developments at millimeter-wave frequencies," *Int. J. Antennas Propag.*, vol. 2016, Oct. 2016, Art. no. 6075680.

[12] R. G. Vaughan and J. B. Andersen, "Antenna diversity in mobile communications," *IEEE Trans. Veh. Technol.*, vol. 36, no. 4, pp. 149–172, Nov. 1987.

[13] B. J. Wysocki, T. A. Wysocki, and J. Seberry, "Modeling dual polarization wireless fading channels using quaternions," in *Proc. Joint IST Workshop Mobile Future, Symp. Trends Commun. (SympoTIC)*, 2006, pp. 68–71.

[14] J. H. Winters, J. Salz, and R. D. Gitlin, "The impact of antenna diversity on the capacity of wireless communication systems," *IEEE Trans. Commun.*, vol. 42, nos. 2–4, pp. 1740–1751, Feb. 1994.

[15] J. Moon and Y. Kim, "Antenna diversity strengthens wireless lans," *Commun. Syst. Des.*, vol. 9, no. 1, pp. 14–22, Jan. 2003.

[16] S. K. Yoo, S. L. Cotton, and W. G. Scanlon, "Switched diversity techniques for indoor off-body communication channels: An experimental analysis and modeling," *IEEE Trans. Antennas Propag.*, vol. 64, no. 7, pp. 3201–3206, Jul. 2016.

[17] L. Zou and C. Fumeaux, "A cross-shaped dielectric resonator antenna for multifunction and polarization diversity applications," *IEEE Antennas Wireless Propag. Lett.*, vol. 10, pp. 742–745, 2011.

[18] B.-J. Liu, J.-H. Qiu, C.-H. Wang, W. Li, and G.-Q. Li, "Polarization-reconfigurable cylindrical dielectric resonator antenna excited by dual probe with tunable feed network," *IEEE Access*, vol. 7, pp. 60111–60119, 2019.

[19] S. K. Podilchak, M. Clenet, and Y. M. M. Antar, "A hybrid dielectric resonator antenna with polarization-agility and wideband operation," in *Proc. 8th Eur. Conf. Antennas Propag. (EuCAP)*, Apr. 2014, pp. 3162–3163.

[20] S. K. Podilchak, J. C. Johnstone, M. Caillet, M. Clenet, and Y. M. M. Antar, "A compact wideband dielectric resonator antenna with a meandered slot ring and cavity backing," *IEEE Antennas Wireless Propag. Lett.*, vol. 15, pp. 909–913, 2016.

[21] W. M. Dyab, A. A. Sakr, and K. Wu, "Dually-polarized butler matrix for base stations with polarization diversity," *IEEE Trans. Microw. Theory Techn.*, vol. 66, no. 12, pp. 5543–5553, Dec. 2018.

[22] J. A. Ruiz-Cruz, M. M. Fahmi, S. A. Fouladi, and R. R. Mansour, "Waveguide antenna feeders with integrated reconfigurable dual circular polarization," *IEEE Trans. Microw. Theory Techn.*, vol. 59, no. 12, pp. 3365–3374, Dec. 2011.

[23] J. Zhang, S. Zhang, Z. Ying, A. S. Morris, and G. F. Pedersen, "Radiation-pattern reconfigurable phased array with p-i-n diodes controlled for 5G mobile terminals," *IEEE Trans. Microw. Theory Techn.*, vol. 68, no. 3, pp. 1103–1117, Mar. 2020.

[24] J. C. Johnstone, S. K. Podilchak, M. Clenet, and Y. M. M. Antar, "A compact cylindrical dielectric resonator antenna for MIMO applications," in *Proc. IEEE Antennas Propag. Soc. Int. Symp. (APSURSI)*, Jul. 2014, pp. 1938–1939.

[25] EETimes. (Jan. 2003). *Antenna Diversity Strengthens Wireless LANs*. [Online]. Available: https://www.eetimes.com/antenna-diversity-strengthens-wireless-lans/

[26] M. Hemalatha, V. Prithiviraj, S. Jayalalitha, and K. Thenmozhii, "Diversity analysis in WiFi system," *J. Theor. Appl. Inf. Technol.*, vol. 33, no. 1, p. 11, Nov. 2011.

[27] S. M. Lindenmeier, L. M. Reiter, D. E. Barie, and J. F. Hopf, "Antenna diversity for improving the BER in mobile digital radio reception especially in areas with dense foliage," in *Proc. 2nd Int. ITG Conf. Antennas*, Mar. 2007, pp. 45–48.

Maksim V. Kuznetcov (Graduate Student Member, IEEE) was born in Kopeysk, Russia, in 1993. He received the M.Eng. degree in electrical and electronic engineering from Heriot-Watt University, Edinburgh, U.K., in 2019. He is currently pursuing the Ph.D. degree at Heriot-Watt University (HWU), Edinburgh, and the University of Edinburgh (UoE), Edinburgh.

In 2019, he joined HWU and UoE as a Research Student, where his research interests include the analysis and design of leaky-wave antennas, duplex and polarization-diverse antenna systems, and other microwave and antenna technologies.

Symon K. Podilchak (Member, IEEE) received the B.A.Sc. degree in engineering science from the University of Toronto, Toronto, ON, Canada, in 2005, the M.A.Sc. and Ph.D. degrees in electrical engineering from Queen's University, Kingston, ON, in 2008 and 2013, respectively, where he received the Outstanding Dissertation Award for his Ph.D.

From 2013 to 2015, he was an Assistant Professor with Queen's University. In 2015, he joined Heriot-Watt University, Edinburgh, U.K., as an Assistant Professor, and became an Associate Professor in 2017. His research is supported by an H2020 Marie Sklodowska-Curie European Research Fellowship. He is currently a Senior Lecturer with the School of Engineering, The University of Edinburgh, Edinburgh. He is also a registered Professional Engineer (P.Eng.) and has had industrial experience as a computer programmer, and has designed 24 and 77 GHz automotive radar systems with Samsung and Magna Electronics. Recent industry experience also includes the design of high-frequency surface-wave radar systems, professional software design, and implementation for measurements in anechoic chambers for the Canadian Department of National Defense and the SLOWPOKE Nuclear Reactor Facility. He has also designed compact antennas for wideband military communications, highly compact circularly polarized antennas for CubeSats with COM DEV International and The European Space Agency (ESA), and, new wireless power transmission systems for Samsung. His research interests include surface waves, leaky-wave antennas, metasurfaces, UWB antennas, phased arrays, and RF integrated circuits.

Dr. Podilchak and his students have been the recipient of many best paper awards and scholarships; most notably Research Fellowships from the IEEE Antennas and Propagation Society (AP-S), the IEEE Microwave Theory and Techniques Society (MTT-S), and the European Microwave Association. He also received a Postgraduate Fellowship from the Natural Sciences and Engineering Research Council of Canada (NSERC) and five Young Scientist Awards from the International Union of Radio Science (URSI). In 2011, 2013, and 2020, student paper awards were received at the IEEE International Symposium on Antennas and Propagation, and in 2012, the Best Paper Prize for Antenna Design at the European Conference on Antennas and Propagation for his work on CubeSat antennas, and in 2016, he received the European Microwave Prize for his research on surface waves and leaky-wave antennas. In 2017 and 2019, he was bestowed a Visiting Professorship Award at Sapienza University, Rome, Italy. He was recognized as an Outstanding Reviewer for the IEEE TRANSACTIONS ON ANTENNAS AND PROPAGATION in 2014 and 2020. He was also the Founder and First Chairman of the IEEE AP-S and IEEE MTT-S Joint Chapters in Kingston, ON, and Scotland. In recognition of these services, he was presented with an Outstanding Volunteer Award in May 2015 from IEEE. He has been a Lecturer for the European School of Antennas and an Associate Editor for *IET Electronics Letters*. Currently, he serves as a Guest Associate Editor for the IEEE OPEN JOURNAL OF ANTENNAS AND PROPAGATION and the IEEE ANTENNAS AND WIRELESS PROPAGATION LETTERS.

Jonathan C. Johnstone (Member, IEEE) was born in North Sydney, NS, Canada. He received the B.Sc. degree (Hons.) in physics from Mount Allison University, Sackville, NB, Canada, in 2011, and the M.A.Sc. degree in electrical engineering from Queen's University, Kingston, ON, Canada, in 2013.

From 2011 to 2013, he was a Research Assistant with Queen's University, where his research was focused on monolithic microwave integrated circuits (ICs) and planar antenna design. In 2013, he was a Research Assistant with The Royal Military College of Canada, Kingston, where his research was focused on dielectric resonator antenna design and radar cross section analysis. Currently, he is working in industry.

Michel Clénet (Senior Member, IEEE) was born in Nantes, France, in 1968. He received the Master in Sciences and Technology (MST) degree in signal processing and the Diplôme d'Études Approfondies (DEA) degree in telecommunications from the University of Rennes I, Rennes, France, in 1991 and 1992 respectively, and the Ph.D. degree in electrical engineering from the University of Nantes, Nantes, France, in 1997.

In 1993, he joined the Electronic and Computer Systems (SEI) Laboratory at IRESTE, Nantes, where he was involved in research on antenna systems for mobile communications. He developed several prototypes for adaptive antenna applications. From 1997 to 1999, he was a Post-Doctoral Fellow at the University of Manitoba, Winnipeg, Canada, where he worked on microstrip antennas, arrays, and horns. Since 1999, he has been with Defense Research and Development Canada (DRDC), Ottawa, Canada, where he has been working on array signal processing, RF systems, planar antennas, arrays, phased arrays, and related technologies, for satellite communication applications. Since 2006, he is leading DRDC activity on controlled reception pattern antenna systems for GPS applications and related technologies. He is authored or coauthored over 15 journal publications and more than 50 communications in international conferences and symposia.

Dr. Clénet is currently an Adjunct Associate Professor at the Royal Military College of Canada and he is Associate Editor for *IET Electronics Letters*. He was the Canadian representative for URSI Commission B from 2012 to 2015.

Yahia M. M. Antar (Life Fellow, IEEE) received the B.Sc. degree (Hons.) from Alexandria University, Alexandria, Egypt, in 1966, and the M.Sc. and Ph.D. degrees from the University of Manitoba, Winnipeg, MB, Canada, in 1971 and 1975, respectively, all in electrical engineering.

In May 1979, he joined the Division of Electrical Engineering, National Research Council of Canada, Ottawa, ON, Canada. In November 1987, he joined the Department of Electrical and Computer Engineering, Royal Military College of Canada, Kingston, ON, where he has been a Professor since 1990. He has authored or coauthored over 200 journal articles, several books, and chapters in books, over 450 refereed conference papers, holds several patents, has chaired several national and international conferences, and has given plenary talks at many conferences.

Dr. Antar was appointed as a member of the Canadian Defense Advisory Board (DAB) of the Canadian Department of National Defense on January 31, 2011. He is a Fellow of the Engineering Institute of Canada (FEIC) and the Electromagnetic Academy. He is also an International Union of Radio Science (URSI) Fellow. In 1977, he held a Government of Canada Visiting Fellowship at the Communications Research Center, Ottawa. In 2003, he was awarded The Royal Military College of Canada "Excellence in Research" Prize and the RMCC Class of 1965 Teaching Excellence award in 2012. He was elected by the URSI to the Board as the Vice President in August 2008 and 2014 and to the IEEE Antennas and Propagation (AP-S) AdCom. In 2019 Professor Antar was elected as the 2020 President-elect for IEEE AP-S, and will serve as its President in 2021. In October 2012, he received the Queen's Diamond Jubilee Medal from the Governor-General of Canada in recognition of his contribution to Canada. He was a recipient of the 2014 IEEE Canada RA Fessenden Silver Medal for Ground Breaking Contributions to Electromagnetics and Communications and the 2015 IEEE Canada J. M. Ham Outstanding Engineering Education Award. In May 2015, he received the Royal Military College of Canada Cowan Prize for excellence in research. He was also a recipient of the IEEE-AP-S of the Chen-To-Tai Distinguished Educator Award in 2017. He served as the Chair for Canadian National Commission (CNC), URSI, from 1999 to 2008, Commission B from 1993 to 1999, and has a cross-appointment at Queen's University, Kingston. In May 2002, he was awarded the Tier 1 Canada Research Chair in electromagnetic engineering which has been renewed in 2016. He has supervised and cosupervised over 90 Ph.D. and M.Sc. theses at the Royal Military College and at Queen's University, several of which have received the Governor-General of Canada Gold Medal Award, the Outstanding Ph.D. Thesis of the Division of Applied Science, as well as many Best Paper Awards in major international symposia. He also has served as an Associate Editor for many IEEE and IET Journals and an IEEE-APS Distinguished Lecturer.